JOURNAL OF NEUROTRAUMA 29:611–619 (February 1, 2012)

DOI: 10.1089/neu.2011.2086

Paranodal Myelin Damage after Acute Stretch in Guinea Pig Spinal Cord

Wenjing Sun,[1] Yan Fu,[2] Yuzhou Shi,[2] Ji-Xin Cheng,[2,3] Peng Cao,[4] and Riyi Shi[1,2]

Abstract

Mechanical injury causes myelin disruption and subsequent axonal conduction failure in the mammalian spinal cord. However, the underlying mechanism is not well understood. In mammalian myelinated axons, proper paranodal myelin structure is crucial for the generation and propagation of action potentials. The exposure of potassium channels at the juxtaparanodal region due to myelin disruption is thought to induce outward potassium currents and inhibit the genesis of the action potential, leading to conduction failure. Using multimodal imaging techniques, we provided anatomical evidence demonstrating paranodal myelin disruption and consequent exposure and redistribution of potassium channels following mechanical insult in the guinea pig spinal cord. Decompaction of paranodal myelin was also observed. It was shown that paranodal demyelination can result from both an initial physical impact and secondary biochemical reactions that are calcium dependent. 4-Aminopyridine (4-AP), a known potassium channel blocker, can partially restore axonal conduction, which further implicates the role of potassium channels in conduction failure. We provide important evidence of paranodal myelin damage, the role of potassium channels in conduction loss, and the therapeutic value of potassium blockade as an effective intervention to restore function following spinal cord trauma.

Key words: calpain; myelin; paranode; potassium channel; secondary injury

Introduction

White matter injury is the most significant contributor to the various levels of disability seen in spinal cord injury (SCI; Blight, 1985; Bunge et al., 1960; Stys, 2004; Totoiu and Keirstead, 2005; Waxman, 1989). It is well known that primary and secondary axonal damage play a significant role in functional loss following SCI. However, it is also possible, although less studied, that acute and persistent myelin damage may also contribute to overall functional loss in SCI. Myelin sheath disruption is a known cause for the loss of axonal conduction seen in mechanical injury (Blight, 1983a; Blight and Decrescito, 1986; Shi and Blight, 1996; Shi and Pryor, 2002). Thus understanding the mechanism of demyelination and the subsequent conduction failure of the surviving, but functionally silent, axons is important not only to ascertain the role of demyelination in functional loss, but also to provide helpful clues for the purpose of eventually establishing potential treatments to restore function after SCI.

Though demyelination has been well documented both immediately following physical impact and in chronic SCI, the mechanism has not been clearly elucidated. SCI consists of two phases: primary injury, referring to the mechanical damage that occurs as a consequence of the physical insult to the nerve tissue, and secondary injury, referring to the chemical injury that occurs immediately following the primary physical insult as a direct result of the mechanical damage. During the phase of secondary injury, the activation of multiple downstream molecular events further injure the spinal cord for days to months following the initial trauma (Blight, 1983b; Blight, 1985; Guest et al., 2005; Lu et al., 2000; Luo et al., 2002a,2002b; Totoiu and Keirstead, 2005; Yamaura et al., 2002). It is well documented that mechanical stress can tear the myelin sheath (Ouyang et al., 2010; Sun et al., 2010), but the precise mechanism responsible for secondary injury to the myelin is not clear. In addition, the differential contribution of primary and secondary injury to demyelination has not been studied in detail in SCI. While physical insults exert an initial instantaneous blow, it takes time for the secondary injury

[1]Department of Basic Medical Sciences, Center for Paralysis Research, [2]Weldon School of Biomedical Engineering, and [3]Department of Chemistry, Purdue University, West Lafayette, Indiana.
[4]Department of Orthopedics, Rui-Jin Hospital, School of Medicine, Shanghai Jiao-tong University, Institute of Trauma and Orthopedics, Shanghai, China.

process to inflict damage. Therefore, understanding secondary demyelination will provide helpful knowledge regarding the therapeutic target and time frame for effective intervention to reduce myelin damage and preserve function.

It has been previously demonstrated that compressive force produced a significant level of stress at the paranodal region during physical deformation, which coincides with severe paranodal myelin disruption in this region (Ouyang et al., 2010). However, the mechanism of secondary myelin damage in such a traumatic injury model has not been studied. The stretch of spinal cord axons is a significant component of compression injury, and stretch injury itself is an important central nervous system (CNS) injury (Blight and DeCrestcito, 1986; Shi and Pryor, 2002). However, paranodal myelin damage has not been studied in detail in stretch injury. The present study aims to investigate the mechanism of acute myelin damage following *ex vivo* stretch injury, especially focusing on the paranodal region. Using an *ex vivo* controlled guinea pig spinal cord stretch injury model (Jensen and Shi, 2003; McBride et al., 2006; Shi and Pryor, 2002), we aimed to determine the differential contribution of primary and secondary injury in myelin disruption during the acute period (0–2 h) post-SCI. With multi-modal imaging techniques we demonstrated immediate paranodal myelin damage and nodal region lengthening following stretch injury. We have also shown that myelin damage can be intensified by secondary injury in a calcium-dependent manner. Such secondary myelin damage can be largely prevented when extracellular calcium was eliminated. This study demonstrates that secondary injury plays an important role in damaging myelin, which suggests a therapeutic opportunity for effective interventions.

Methods

Animals

With the approval of the Purdue Animal Care and Use Committee (PACUC), adult female guinea pigs (300–450 g) were anesthetized with a ketamine (80 mg/kg), xylazine (12 mg/kg), and acepromazine (0.8 mg/kg) mixture. Following anesthesia the spinal cord was extracted as previously described (Shi and Blight, 1996; Shi and Borgens, 2000; Shi and Pryor, 2002), and was then incubated in oxygenated Krebs' solution (124 mM NaCl, 2 mM KCl, 1.2 mM KH_2PO_4, 1.3 mM $MgSO_4$, 2 mM $CaCl_2$, 10 mM dextrose, 26 mM $NaHCO_3$, and 10 mM sodium ascorbate).

Stretch injury

Ex vivo stretch injury to isolated guinea pig spinal cord ventral white matter strips was induced by the method reported in previous studies (Jensen and Shi, 2003; Shi and Pryor, 2002). In brief, 4.5-cm spinal cord strips were placed in a modified double sucrose gap chamber (Fig. 1A). Nylon mesh was placed on top of the strip for stabilization. A stretch rod fell from a predetermined height into the hole of central compartment and induced stretch injury to the spinal cord strip (Fig. 1B). The stretch rod was released immediately after inducing the stretch injury. For electrophysiological recording, a double sucrose gap chamber was used to monitor the real-time compound action potential (CAP) as an assessment of conduction function (Shi and Blight, 1996,1997; Shi and Borgens, 2000). For anatomical study, a 1-cm segment was cut from the epicenter of the injury site immediately after stretch and examined by imaging methods. As shown in Figure 1B, the 1-cm segment in the middle of the spinal cord sample was uniformly stretched. For the Ca^{2+} removal group, the spinal cord samples were dissected out and immediately incubated in Ca^{2+}-free Krebs' solution prior to injury, and remained in Ca^{2+}-free Krebs' solution during the injury procedure and for the following 2 h. The control group consists of the spinal cord sample dissected out and incubated in Krebs' solution without stretch injury before fixation. The length of incubation time was the same as for the corresponding stretch group.

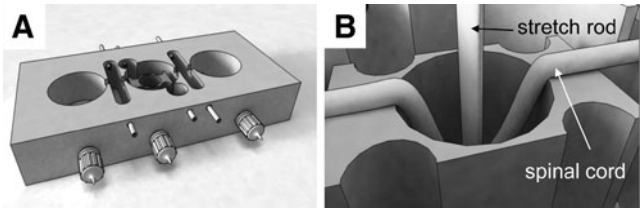

FIG. 1. Illustration of the modified double-sucrose gap chamber for our *ex-vivo* stretch injury model. (**A**) Drawing shows the 3D construction of the recording chamber. In the central compartment there was a stage with a built-in hole. (**B**) This drawing depicts a spinal cord sample being stretched by a stretch rod.

Transmission electron microscopy (TEM) imaging

One centimeter of spinal cord ventral white matter tissue within the injury area was fixed in 3% glutaraldehyde for 30 min and cut into 1×2-mm blocks. The blocks continued fixation in 3% glutaraldehyde for 1 h, followed by fixation in 2% osmium tetroxide for 1 h. All the fixatives were made with 0.1 M cacodylate buffer. After washing, the blocks were dehydrated in a graded ethanol series and then embedded in Epon Generic Resin. The sections with a thickness of about 90 nm were prepared with uranyl acetate and lead citrate stain and examined with a transmission electron microscope.

Coherent anti-Stokes Raman scattering imaging (CARS) and immunofluorescence imaging

Coherent anti-Stokes Raman scattering (CARS) microscopy was utilized for label-free imaging of the myelin sheath in spinal cord white matter as previously reported (Fu et al., 2007; Wang et al., 2005). In each experimental group, 5 spinal cord tissue samples from 5 different animals were used for quantification. Specifically, one strip of spinal cord ventral white matter (4.5 cm) was dissected out from each animal. Only one segment (1 cm) from the injury epicenter was collected from each strip for CARS analysis. The spinal cord samples were fixed in 4% paraformaldehyde overnight and then directly imaged by CARS microscopy. For the purpose of identifying and examining the node using CARS imaging, we collected the image of every single node of Ranvier that we encountered until the number for one sample reached 20–25. The imaging field was randomly chosen within the stretch area. The person that conducted the image analysis was different than the person that performed the stretch injury and was unaware of the identity of the specimen. Node ratio was calculated as node length over axon diameter as previously

described (Fu et al., 2009; Fig. 3E). Node ratios were compared among various experimental groups.

For immunofluorescence labeling, 1 cm of spinal cord tissue was fixed in 4% paraformaldehyde for 24 h and followed by cryoprotection in 20% glycerol for 48 h. The tissue was then cut into 50-μm sections using an oscillating tissue slicer (OTS-4000; Electron Microscopy Sciences, Hatfield, PA). After blocking with 5% bovine serum albumin (BSA) and 0.5% Triton X-100 for 1 h, the sections were incubated with primary antibody overnight at 4°C. Rabbit-raised anti-Kv1.2 (dilution ratio 1:100; Alomone Labs Ltd., Jerusalem, Israel) and rabbit-raised anti-Caspr (dilution ratio 1:100, the monoclonal antibody was obtained from the University of California–Davis/National Institutes of Health [NIH] NeuroMab Facility, supported by NIH grant U24NS050606 and maintained by the Department of Neurobiology, Physiology and Behavior, College of Biological Sciences, University of California–Davis) were used in this study. The sections were incubated in the secondary antibody, Alexa-Fluor® 488 conjugated goat anti-rabbit IgG (H + L; Invitrogen, Carlsbad, CA) for 1 h at room temperature. Two-photon excited fluorescence (TPEF) imaging of labeled proteins was performed simultaneously with CARS imaging at the same platform.

Chemical agents

First, 10 μM of nimodipine (Sigma-Aldrich, St. Louis, MO) and 100 μM $CdCl_2$ (Sigma-Aldrich) were both freshly made. Spinal cord samples were pre-incubated with nimodipine or $CdCl_2$ for 1 h before the experiments. Then 500 μM of calpain inhibitor III (Calbiochem, La Jolla, CA) was freshly made and pre-incubated with spinal cord samples for 30 min prior to the experiment.

Statistical analysis

One way analysis of variance (ANOVA) and Tukey's *post-hoc* tests were used for comparison of node ratios for multiple groups. The paired Student's *t*-test was used to compare CAP amplitudes between pre- and post-treatment with 4-AP. All data are expressed as mean ± standard error of the mean (SEM).

Results

Paranodal myelin damage following acute stretch injury

The structural change of the myelin sheath after acute stretch injury was first investigated by TEM. In the normal tissue without injury, paranodal myelin was observed to tightly cover the axon and connected with axolemma by axonal-glial junctions (Fig. 2A and B). In the post-stretch injury tissue (t = 0 and t = 2 h), paranodal myelin disruption (Fig. 2C, D, E, and F) was observed. Specifically, in the samples immediately post-injury (t = 0), noticeable elongated nodes were observed (Fig. 2C and D). In addition, severe de-compaction or loosening of the myelin lamella in the paranodal region was also noted. At 2 h post-stretch injury, the detachment of paranodal myelin from the axon membrane (Fig. 2E and F) was commonly observed.

To further confirm the paranodal myelin disruption and quantify the node region lengthening, we utilized label-free CARS microscopy to characterize the structure of paranodal myelin. Figure 3A shows a CARS image of a normal node of Ranvier in a control sample. In the 3 post-injury groups: group I (immediately post-stretch), group II (2 h post-stretch), and group III (2 h post stretch + Ca^{2+}-free solution), conspicuous lengthening of the node region (Fig. 3B, C, and D) was commonly observed in the CARS images. For quantifying the node region lengthening, we used node ratio, which is defined as the value of the node length divided by axon diameter (Fig. 3E). All 3 post-injury groups had significantly higher values of node ratios (group I, 1.84 ± 0.12, $n = 77$; group II, 2.71 ± 0.18, $n = 102$; group III, 1.73 ± 0.15, $n = 89$) compared to controls (0.83 ± 0.07, $n = 131$, $p < 0.001$ for all three comparisons). Moreover, group II had a significantly higher node ratio than group I ($p < 0.05$). However, when we eliminated the Ca^{2+} from the Krebs' solution, the further nodal lengthening observed in group II

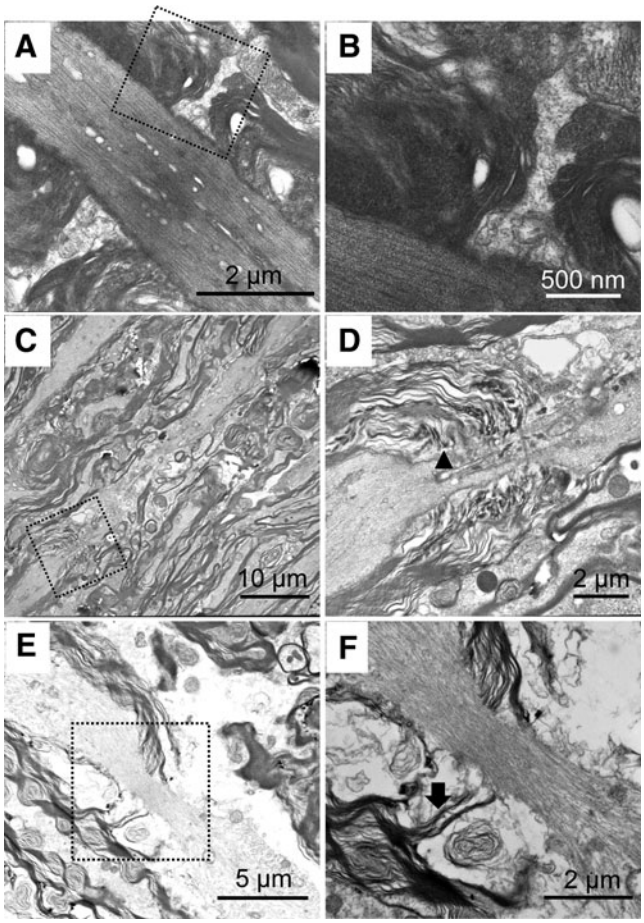

FIG. 2. Paranodal myelin damage was observed following acute stretch injury by transmission electron microscopy (TEM). The right panel images (**B**, **D**, and **F**) are the magnified images of the dashed boxes in the left panels (**A**, **C**, and **E**). (**A** and **B**) In normal spinal cord tissue, paranodal myelin was tightly connected with axolemma. (**C** and **D**) In spinal cord tissue that was immediately fixed after stretch injury, the node region was noticeably elongated. Also, there were signs of myelin de-compaction in the paranodal myelin-axolemma conjunction area (arrowhead in **D**), which indicates paranodal myelin disruption (**E** and **F**). When the tissue was fixed 2 h after stretch injury, the detachment of paranodal myelin (arrow) from the axon membrane was observed.

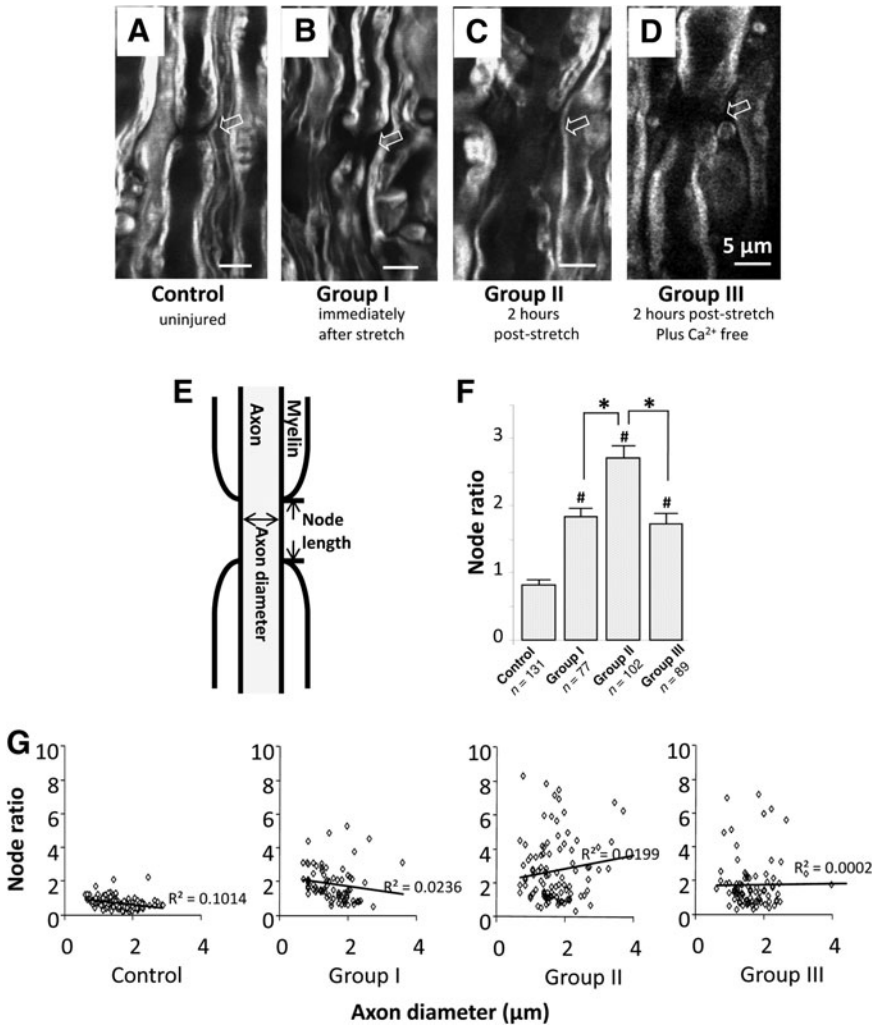

FIG. 3. Coherent anti-Stokes Raman scattering (CARS) imaging demonstrated paranodal myelin splitting and retraction in the stretch-injured spinal cord. Micrographs show the CARS images taken in four conditions: control (**A**), immediate fixation after stretch injury (**B**, group I), fixation at 2 h post-injury (**C**, group II), and 2 h post-injury incubated in Ca^{2+}-free Krebs' solution (**D**, group III). Arrows indicate the node regions. For quantification, we defined the node ratio as the ratio of node length over axon diameter (scale bars = 5 μm in **A**–**D**). The method of determining node length and axon diameter is illustrated in **E**. (**F**) Bar graph showing the node ratio quantification for the four experimental groups: control, 0.83 ± 0.07 ($n = 131$); group I (immediate fixation after injury), 1.84 ± 0.12 ($n = 77$); group II (2 h post-injury), 2.71 ± 0.18 ($n = 102$); and group III (Ca^{2+}-free 2 h post-injury), 1.73 ± 0.15 (n = 89). All three post-injury groups had significantly larger node ratios than controls ($p < 0.001$ for all three groups). Group II had a larger node ratio than group I ($p < 0.05$). Group III also had a significantly smaller node ratio than group II ($p < 0.05$). There was no significant difference between group I and group III (#$p < 0.001$ compared to controls; *$p < 0.05$). (**G**) Scatterplots of node ratios against axon diameters for all 4 groups. The correlations between node ratio and axon diameter were weak in the control and experimental groups (shown as R values).

was diminished (group III in Fig. 3F). These results strongly suggest that the paranodal myelin disruption results from both primary injury and secondary injury within 2 h post -stretch and in a Ca^{2+}-dependent manner. It is worth noting that the correlations between node ratio and axon diameter are weak in all four groups (Fig. 3G).

The calpain activation pathway is involved in secondary injury mechanisms

Since extracellular calcium influences axonal myelin degradation and the site of action is likely intracellular, we investigated how Ca^{2+} gains access to the intra-axonal space after injury. We examined the effect of two calcium channel blockers, nimodipine (an L-type calcium channel blocker) and cadmium (a broad-spectrum calcium channel blocker), on node ratio in cord samples 2 h post-stretch. The results showed that neither calcium channel blocker significantly reduced the increase in node ratio examined 2 h post-stretch (Fig. 4A, $p > 0.05$), although cadmium showed a slightly increased tendency to reduce the node ratio. This indicates that calcium does not enter the intracellular space through voltage-dependent calcium channels. Therefore, it is likely that calcium influx is mainly through non-specific membrane disruptions induced by stretch injury and other biochemical agents (Shi and Whitebone, 2006; Shi et al., 2002).

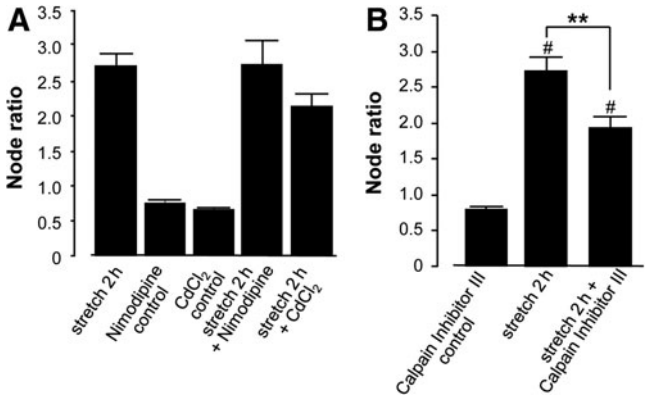

FIG. 4. (**A**) When calcium channel blockers (10 μM nimodipine and 100 μM cadmium) were applied in the 2-h post-stretch group the node ratio was not significantly changed ($p > 0.05$) compared to stretch without these agents. Neither nimodipine nor cadmium altered the node ratio in uninjured samples ($p > 0.05$). (**B**) Inhibition of calpain reduced the increase in node ratio seen at 2 h post-injury. A dose of 500 μM of calpain inhibitor III was applied 30 min before stretch injury. The samples were fixed 2 h after injury. Compared to stretched tissue in normal Krebs' solution, the calpain inhibitor III significantly reduced the node ratio, from 2.71 ± 0.18 (as shown in Fig. 3) to 1.92 ± 0.16 ($n = 102$, $^{**}p < 0.05$, $^{\#}p < 0.05$ compared to control). Calpain inhibitor III did not cause significant changes in node ratio in uninjured samples ($p > 0.05$).

Calpain is a calcium-dependent protease that is involved in many damaging processes, including those related to myelin degradation (Bartus et al., 1994; Demarchi and Schneider, 2007; Li et al., 1998; Shulga and Pastorino, 2006). To examine whether calpain activation is involved in the secondary myelin damage seen post-stretch, we added a calpain inhibitor III to the Krebs' solution bathing the spinal cord before the injury and examined the samples 2 h after injury. The analysis of CARS images (Fig. 5B) showed that the calpain inhibitor III significantly reduced node ratio at 2 h post-stretch (1.92 ± 0.16, $n = 102$) compared to samples without the calpain inhibitor (2.70 ± 0.18, $n = 102$, $p < 0.01$). This indicates that calpain plays a significant role in post-stretch secondary myelin damage.

Paranodal conjunction dissociation following stretch injury

The paranodal conjunction complex is a structure that connects myelin with the axonal membrane at the paranodal region (Bhat et al., 2001; Dupree et al., 1999; Poliak and Peles, 2003). In order to investigate the alteration of the paranodal conjunction complex structure following stretch injury, we used anti-Caspr to label axonal membrane protein Caspr, an integral component of the paranodal conjunction complex, and CARS to visualize the myelin sheath. It is clear that in healthy control spinal cord tissue the Caspr signal was largely covered by the paranodal myelin sheath (Fig. 5A–C). This is consistent with the notion that the paranodal conjunction complex holds the axonal membrane together with myelin (Poliak and Peles, 2003). In stretch-injured tissue, however, the paranodal myelin signals were dissociated and retracted away from Caspr (Fig. 5D–F). This indicates that stretch injury-induced damage resulted in the disconnection of myelin from the axonal membrane.

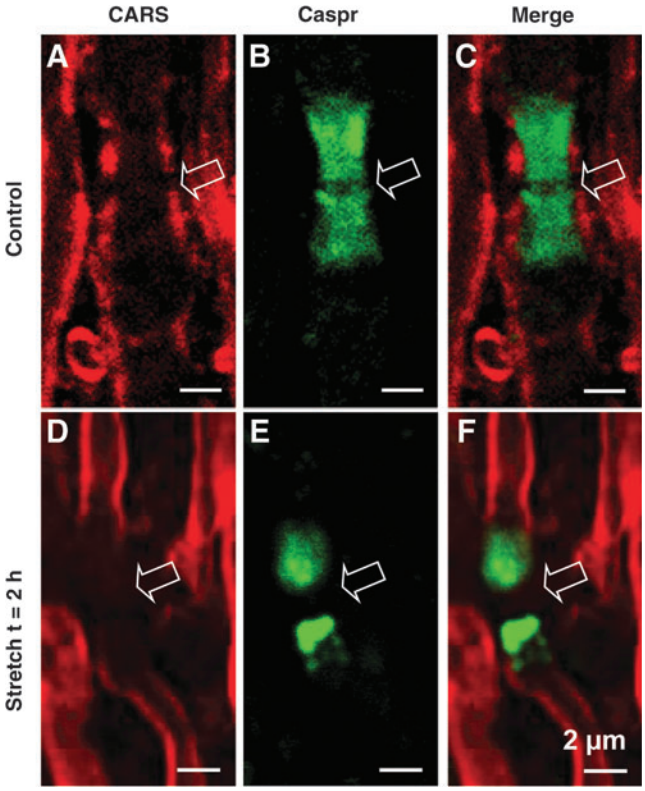

FIG. 5. Coherent anti-Stokes Raman scattering (CARS) imaging of myelin and two-photon excited fluorescence (TPEF) imaging of paranodal Caspr in stretch-injured spinal cord. (**A** and **D**) Photomicrographs show CARS images of myelin sheaths (shown in red). (**B** and **E**) Images of immunofluorescent labeling of Caspr (shown in green). (**C** and **F**) Merged CARS and TPEF images. In normal tissue, the paranodal myelin sheath signal was aligned with Caspr staining (**C**). In 2-h post-stretch injury tissue, the myelin sheath was retracted from the paranodal region and was dissociated from Caspr labeling (**F**; scale bars = 2 μm). Color image is available at www.liebertonline.com/neu

Exposure and redistribution of juxtaparanodal potassium channels after stretch injury

The potassium channels normally cluster at the juxtaparanodal area underneath the myelin sheath (Bhat et al., 2001; Poliak et al., 2003; Rasband and Trimmer, 2001; Vabnick and Shrager, 1998; Fig. 6A, B, and C). Exposure and activation of potassium channels in demyelinated axons plays an important role in conduction block following spinal cord trauma. However, clear morphological evidence of potassium channel exposure in acute spinal cord trauma is still not well established. In order to provide such evidence and observe its dynamic changes following acute demyelination, we used anti-$K_v1.2$ antibody to label potassium channels located at the juxtaparanodal region. In addition, we also performed simultaneous CARS imaging and TPEF imaging to visualize myelin and immune-labeled potassium channels, respectively. This allowed us to examine the paranodal myelin disruption and the consequent exposure of potassium channels in reference to myelin in acute stretch injury. As shown in Figure 6, 2 h after stretch injury, there was clear paranodal myelin retraction towards the internodal region and partial

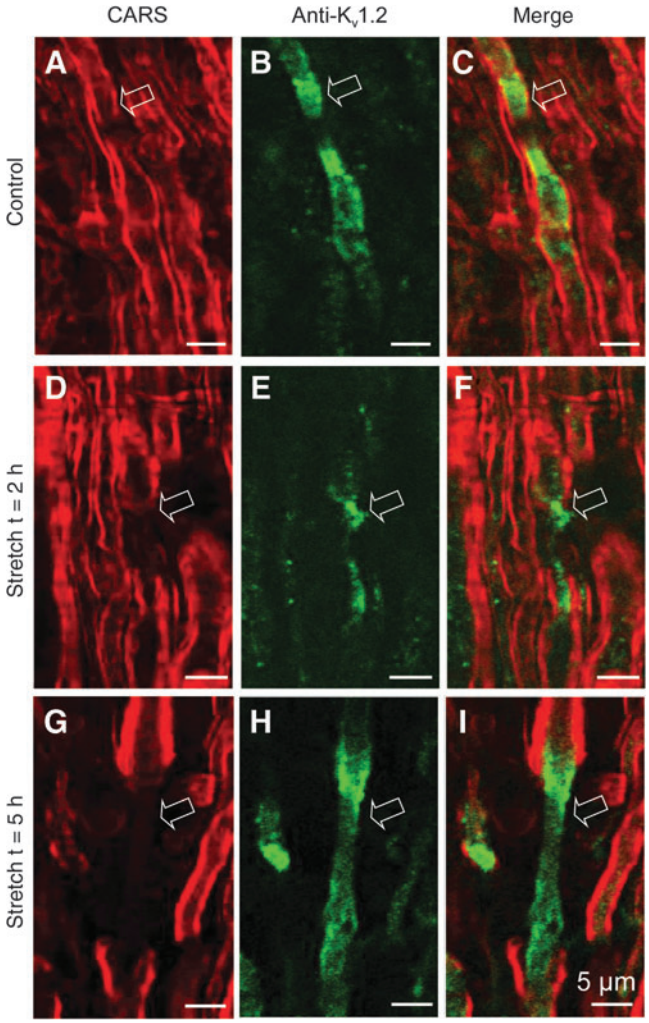

FIG. 6. K_v1.2 channels were exposed due to paranodal myelin retraction following acute stretch injury. (**A**, **D** and **G**) Coherent anti-Stokes Raman scattering (CARS) images revealed significant and graded lengthening of the node region and obvious retraction of paranodal myelin (shown in red) post-stretch injury (**D** and **G**) compared to controls (**A**). (**B**, **E**, and **H**) Photomicrographs illustrating TPEF imaging of K_v1.2 channels (shown in green). (**C**, **F**, and **I**) Merged images of CARS and TPEF. In normal tissue, K_v1.2 channels were observed to cluster in the juxtaparanodal region covered by myelin (**C**). Two hours after stretch injury, K_v1.2 channels were exposed due to paranodal myelin retraction (**F**). Five hours after stretch injury, K_v1.2 channels migrated to the node region (**I**). Arrows point to the node regions (scale bars = 5 μm). Color image is available at www.liebertonline.com/neu

exposure of K_v1.2 channels (Fig. 6D, E, and F). The myelin retraction and exposure of potassium channels was more pronounced at 5 h after stretch injury. In addition, redistribution of K_v1.2 channels toward the node region was distinct, as this area lacks potassium channels under normal conditions (Fig. 6A, B, C, G, H, and I).

4-Aminopyridine (4-AP) increased impulse conduction in stretch-injured spinal cord tissue

Compound action potential (CAP) conduction in the spinal cord ventral white matter strip was examined using a double-sucrose gap recording system. After initial stabilization, acute stretch injury was performed and the CAP amplitude initially decreased, and then recovered slowly but steadily. When CAP recovery was stabilized, 100 μM of 4-AP was applied to the injured spinal cord. As shown in Figure 7A and B, 4-AP increased CAP amplitude of the injured spinal cord, from 0.29 ± 0.08 mV to 0.42 ± 0.11 mV ($n = 7$, $p < 0.05$). This result is consistent with the notion that paranodal myelin disruption results in potassium channel exposure, leading to conduction block.

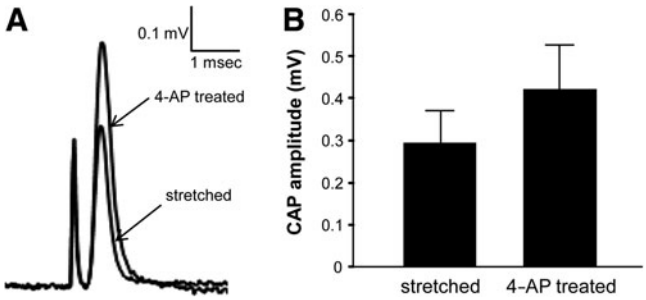

FIG. 7. 4-Aminopyridine (4-AP) restored action potential conduction in the spinal cord post-stretch injury. (**A**) The representative compound action potential (CAP) recorded from stretched spinal cord before 4-AP treatment was superimposed onto the CAP recorded from the same spinal cord sample with 4-AP treatment. (**B**) Graph illustrating that 100 μM of 4-AP significantly increased CAP amplitude, from 0.29 ± 0.08 mV to 0.42 ± 0.11 mV ($n = 7$, $p < 0.05$).

Discussion

In this study we showed that there are at least two components of myelin disruption as a result of mechanical injury to the spinal cord. Demyelination can be produced by primary physical impact (primary demyelination), and by secondary biochemical events (secondary demyelination). A calcium-dependent degenerative process appears to be involved in secondary myelin disruption in the acute phase (as early as 2 h) following longitudinal stretch of the spinal cord. The findings show that separating primary and secondary myelin damage in neurotrauma is possible. This knowledge will facilitate the understanding of the mechanism of demyelination in acute SCI, and may suggest effective interventions to reduce myelin damage, a component of SCI pathology with proven functional consequences.

Paranodal myelin disruption, such as nodal region lengthening, as a result of myelin retraction is the chief observation of myelin damage in the present study, and was supported by evidence from both TEM and CARS images. Additionally, quantitative analysis demonstrated that myelin damage at 2 h post-injury is almost twice as severe as the damage seen immediately following injury, as estimated from nodal ratio quantification (Fig. 3F). This finding indicates that primary injury results from the initial mechanical insult, and only contributed partially to the paranodal myelin disruption seen 2 h post-injury. Further, this suggests that secondary injury can significantly exacerbate myelin damage, and more importantly, paranodal myelin retraction can in part be prevented in our experimental setting. Specifically, it was possible to block the secondary myelin damage

by bathing the cord samples in calcium-free Krebs' solution. As calcium is a well-known mediator for various cascades of reactions in secondary injury, this finding seems to suggest that calcium-dependent secondary injury mechanisms play a role in myelin damage as early as 2 h following spinal cord trauma. These findings also indicate that the source of calcium is mainly from the extracellular space, although an intracellular source cannot be ruled out completely based on the current study. The two voltage-dependent calcium channel blockers, nimodipine and $CdCl_2$, had minimal influence on the myelin damage. This indicates that voltage-dependent calcium channels do not play a major role in mediating calcium influx following stretch injury. Other avenues, such as non-specific leakages due to membrane damage, may be dominant factors in this case (Shi and Whitebone, 2006; Shi et al., 2002).

The paranodal septate junction is an axonal-glial protein complex that is comprised of contactin-associated protein (Caspr), Nfac 155, contactin, spectrin, protein 4.1, and actin (Bhat, 2003; Bhat et al., 2001; Girault and Peles, 2002; Gollan et al., 2003; Ogawa et al., 2006; Poliak and Peles, 2003; Susuki and Rasband, 2008). Both protein 4.1 and spectrin are known calpain substrates (Goll et al., 2003), and calpain itself is a calcium-dependent protease. Thus it is likely that calpain activation caused by calcium influx leads to degradation of protein 4.1 and spectrin, exacerbating further paranodal junction interruption and myelin retraction. This hypothesis is supported by the finding that the calpain inhibitor III prevented further paranodal myelin retraction and therefore alleviated myelin damage (Fig. 4B). The fact that neither the calpain inhibitor nor the voltage-dependent calcium channel blockers had a significant effect on myelin structure in the normal uninjured axons of the control group indicates that calcium-mediated protease activation plays a minor role in the short-term maintenance of myelin health.

Asymmetrical distribution of ion channels at the nodal and paranodal regions is important for maintenance of saltatory conduction in myelinated axons (Poliak and Peles, 2003; Rasband and Trimmer, 2001). In contrast to voltage-dependent sodium channels, which are strictly located within the node of Ranvier, voltage-gated potassium channels ($K_v1.1$, 1.2, and β2.1) are clustered at the juxtaparanodal region and are covered by the myelin sheath under normal conditions (Arroyo and Scherer, 2000; Rasband and Trimmer, 2001; Vabnick and Shrager, 1998). Proper axonal-glial junction structure prevents potassium channels from migrating into the node region, ensuring that they remain underneath the myelin and do not interfere with normal conduction generation or propagation at the node region. Previous reports demonstrate that acute stretch injury exposes juxtaparanodal potassium channels (Sun et al., 2010). In the current study, we expanded on this conclusion by investigating two time points post-injury, 2 h and 5 h. At 2 h post-injury we observed exposure of potassium channels (Fig. 6D–F), which is consistent with previous findings (Sun et al., 2010). However, at 5 h post-injury, we noted a significant redistribution of potassium channels into the nodal region (Fig. 6G–I). Similar redistribution of potassium channels has been previously reported in chronic spinal cord injury (Karimi-Abdolrezaee et al., 2004; Nashmi et al., 2000) and multiple sclerosis (Howell et al., 2006). However, the defining factor of the current study is that the exposure and migration of the voltage-dependent potassium channels was observed in reference to myelin structure, which was imaged simultaneously using a label-free CARS technique. The novel imaging technique of CARS is instrumental in allowing imaging of the myelin structure in addition to immune-labeled potassium channels, so the misalignment of paranodal myelin and potassium channels can be confirmed. Therefore, by using immunofluorescence staining and CARS simultaneously, we provided direct evidence that potassium channels were indeed exposed and redistributed following mechanical injury, a phenomenon with severe functional consequences.

We postulated that potassium channel redistribution started from the paranodal region. The initial mechanical injury and consequent secondary injury interrupted the paranodal axonal-glial junction and removed the physical barrier so that potassium channels were first exposed, and then migrated into the nodal region. The evidence obtained from electrical impulse conduction assessment further supported our hypothesis. 4-AP is a well-known potassium channel blocker. In the current study when 100 μM of 4-AP was applied to spinal cord samples following stretch injury, the CAP amplitude increased by more than 40% (Fig. 7). This result is consistent with other studies showing that 4-AP restores axonal conduction following mechanical damage and myelin disruption in the spinal cord (Blight, 1989; Jensen and Shi, 2003; Shi and Blight, 1997). One possible reason that 4-AP only partially restores conduction is that some of the axons that suffered myelin damage also suffered axonal membrane disruption, compromising the integrity of both structures which are indispensible in neuronal function. In support of such a notion, there is widespread membrane damage following spinal cord mechanical trauma (Shi, 2004; Simon et al., 2009), and compounds that are known to seal membrane disruption, such as polyethylene glycol, can also restore axonal conduction (Donaldson et al., 2002; Shi and Borgens, 2000).

In summary, we demonstrated that paranodal myelin disruption and retraction is a significant component of the pathology of acute spinal cord stretch injury. Both primary and secondary injuries contribute to paranodal myelin disruption and subsequent conduction failure. The secondary injury begins within 2 h of initial stretch, and largely occurred through a calcium- and calpain-dependent manner. Finally, our results provide pertinent anatomical evidence supporting the role of potassium channels in the conduction block associated with spinal cord injury. Through the simultaneous use of CARS and TPEF imaging modalities we were able to visualize both the exposure and redistribution of $K_v1.2$ channels post-stretch injury. The subsequent restoration of CAP conduction with 4-AP treatment in the stretched spinal cords further indicates that fast potassium channels are a major culprit in conduction loss, and may represent an effective therapeutic target for clinical interventions in the myelin-related pathology associated with spinal cord injury.

Acknowledgments

The authors would like to thank Sean Connell and Melissa Tully for critical reading of the manuscript, and Michel Schweinsberg for drawing the illustrations. We would also like to acknowledge the financial support from the NIH, and a

grant (09410706000) provided by the Science and Technology Commission of Shanghai Municipality, Shanghai, China.

Author Disclosure Statement

No competing financial interests exist.

References

Arroyo, E.J., and Scherer, S.S. (2000). On the molecular architecture of myelinated fibers. Histochem. Cell Biol. 113, 1–18.

Bartus, R.T., Baker, K.L., Heiser, A.D., Sawyer, S.D., Dean, R.L., Elliott, P.J., and Straub, J.A. (1994). Postischemic administration of AK275, a calpain inhibitor, provides substantial protection against focal ischemic brain damage. J. Cereb. Blood Flow Metab. 14, 537–544.

Bhat, M.A. (2003). Molecular organization of axo-glial junctions. Curr. Opin. Neurobiol. 13, 552–559.

Bhat, M.A., Rios, J.C., Lu, Y., Garcia-Fresco, G.P., Ching, W., St Martin, M., Li, J., Einheber, S., Chesler, M., Rosenbluth, J., Salzer, J.L., and Bellen, H.J. (2001). Axon-glia interactions and the domain organization of myelinated axons requires neurexin IV/Caspr/Paranodin. Neuron 30, 369–383.

Blight, A.R., and Decrescito, V. (1986). Morphometric analysis of experimental spinal cord injury in the cat: the relation of injury intensity to survival of myelinated axons. Neuroscience 19, 321–341.

Blight, A.R. (1983a). Axonal physiology of chronic spinal cord injury in the cat: intracellular recording in vitro. Neuroscience 10, 1471–1486.

Blight, A.R. (1983b). Cellular morphology of chronic spinal cord injury in the cat: analysis of myelinated axons by line-sampling. Neuroscience 10, 521–543.

Blight, A.R. (1985). Delayed demyelination and macrophage invasion: a candidate for secondary cell damage in spinal cord injury. Cent. Nerv. Syst. Trauma 2, 299–315.

Blight, A.R. (1989). Effect of 4-aminopyridine on axonal conduction-block in chronic spinal cord injury. Brain Res. Bull. 22, 47–52.

Bunge, R.P., Bunge, M.B., and Ris, H. (1960). Electron microscopic study of demyelination in an experimentally induced lesion in adult cat spinal cord. J. Biophys. Biochem. Cytol. 7, 685–696.

Demarchi, F., and Schneider, C. (2007). The calpain system as a modulator of stress/damage response. Cell Cycle 6, 136–138.

Donaldson, J., Shi, R., and Borgens, R. (2002). Polyethylene glycol rapidly restores physiological functions in damaged sciatic nerves of guinea pigs. Neurosurgery 50, 147–156; discussion 156–147.

Dupree, J.L., Girault, J.A., and Popko, B. (1999). Axo-glial interactions regulate the localization of axonal paranodal proteins. J. Cell Biol. 147, 1145–1152.

Fu, Y., Sun, W., Shi, Y., Shi, R., and Cheng, J.X. (2009). Glutamate excitotoxicity inflicts paranodal myelin splitting and retraction. PLoS One 4, e6705.

Fu, Y., Wang, H., Huff, T.B., Shi, R., and Cheng, J.X. (2007). Coherent anti-Stokes Raman scattering imaging of myelin degradation reveals a calcium-dependent pathway in lyso-PtdCho-induced demyelination. J. Neurosci. Res. 85, 2870–2881.

Girault, J.A., and Peles, E. (2002). Development of nodes of Ranvier. Curr. Opin. Neurobiol. 12, 476–485.

Gollan, L., Salomon, D., Salzer, J.L., and Peles, E. (2003). Caspr regulates the processing of contactin and inhibits its binding to neurofascin. J. Cell Biol. 163, 1213–1218.

Goll, D.E., Thompson, V.F., Li, H., Wei, W., and Cong J. (2003). The calpain system. Physiol. Rev. 83, 731–801.

Guest, J.D., Hiester, E.D., and Bunge R.P. (2005). Demyelination and Schwann cell responses adjacent to injury epicenter cavities following chronic human spinal cord injury. Exp. Neurol. 192, 384–393.

Howell, O.W., Palser, A., Polito, A., Melrose, S., Zonta, B., Scheiermann, C., Vora, A.J., Brophy, P.J., and Reynolds R. (2006). Disruption of neurofascin localization reveals early changes preceding demyelination and remyelination in multiple sclerosis. Brain 129, 3173–3185.

Jensen, J.M., and Shi, R. (2003). Effects of 4-aminopyridine on stretched mammalian spinal cord: the role of potassium channels in axonal conduction. J. Neurophysiol. 90, 2334–2340.

Karimi-Abdolrezaee, S., Eftekharpour, E., and Fehlings, M.G. (2004). Temporal and spatial patterns of Kv1.1 and Kv1.2 protein and gene expression in spinal cord white matter after acute and chronic spinal cord injury in rats: implications for axonal pathophysiology after neurotrauma. Eur. J. Neurosci. 19, 577–589.

Li, P.A., Howlett, W., He, Q.P., Miyashita, H., Siddiqui, M., and Shuaib, A. (1998). Postischemic treatment with calpain inhibitor MDL 28170 ameliorates brain damage in a gerbil model of global ischemia. Neurosci. Lett. 247, 17–20.

Lu, J., Ashwell, K.W., and Waite, P. (2000). Advances in secondary spinal cord injury: role of apoptosis. Spine (Phila. Pa. 1976) 25, 1859–1866.

Luo, J., Li, N., Robinson, P.J., and Shi, R. (2002a). Detection of reactive oxygen species by flow cytometry after spinal cord injury. J. Neurosci. Methods 120, 105–112.

Luo, J., Li, N., Robinson, P.J., and Shi, R. (2002b) The increase of reactive oxygen species and their inhibition in an isolated guinea pig spinal cord compression model. Spinal Cord 40, 656–665.

McBride, J.M., Smith, D.T., Byrn, S.R., Borgens, R.B., and Shi, R. (2006). Dose responses of three 4-aminopyridine derivatives on axonal conduction in spinal cord trauma. Eur. J. Pharm. Sci. 27, 237–242.

Nashmi, R., Jones, O.T., and Fehlings, M.G. (2000). Abnormal axonal physiology is associated with altered expression and distribution of Kv1.1 and Kv1.2 K+ channels after chronic spinal cord injury. Eur. J. Neurosci. 12, 491–506.

Ogawa, Y., Schafer, D.P., Horresh, I., Bar, V., Hales, K., Yang, Y., Susuki, K., Peles, E., Stankewich, M.C., and Rasband, M.N. (2006). Spectrins and ankyrinB constitute a specialized paranodal cytoskeleton. J. Neurosci. 26; 5230–5239.

Ouyang, H., Sun, W., Fu, Y., Li, J., Cheng, J.X., Nauman, E., and Shi, R. (2010). Compression induces acute demyelination and potassium channel exposure in spinal cord. J. Neurotrauma 27, 1109–1120.

Poliak, S., and Peles, E. (2003). The local differentiation of myelinated axons at nodes of Ranvier. Nat. Rev. Neurosci. 4, 968–980.

Poliak, S., Salomon, D., Elhanany, H., Sabanay, H., Kiernan, B., Pevny, L., Stewart, C.L., Xu, X., Chiu, S.Y., Shrager, P., Furley, A.J., and Peles, E. (2003). Juxtaparanodal clustering of Shaker-like K+ channels in myelinated axons depends on Caspr2 and TAG-1. J. Cell Biol. 162, 1149–1160.

Rasband, M.N., and Trimmer, J.S. (2001). Developmental clustering of ion channels at and near the node of Ranvier. Dev. Biol. 236, 5–16.

Shi, R., and Blight, A.R. (1996). Compression injury of mammalian spinal cord in vitro and the dynamics of action potential conduction failure. J. Neurophysiol. 76, 1572–1580.

Shi, R., and Blight, A.R. (1997). Differential effects of low and high concentrations of 4-aminopyridine on axonal conduction in normal and injured spinal cord. Neuroscience 77, 553–562.

Shi, R., and Borgens, R.B. (2000). Anatomical repair of nerve membranes in crushed mammalian spinal cord with polyethylene glycol. J. Neurocytol. 29, 633–643.

Shi, R., and Pryor, J.D. (2002). Pathological changes of isolated spinal cord axons in response to mechanical stretch. Neuroscience 110, 765–777.

Shi, R., Luo, J., and Peasley, M.A. (2002) Acrolein inflicts axonal membrane disruption and conduction loss in isolated guinea pig spinal cord. Neuroscience 115, 337–340.

Shi, R., and Whitebone, J. (2006). Conduction deficits and membrane disruption of spinal cord axons as a function of magnitude and rate of strain. J. Neurophysiol. 95, 3384–3390.

Shi, R. (2004). The dynamics of axolemmal disruption in guinea pig spinal cord following compression. J. Neurocytol. 33, 203–211.

Shulga, N., and Pastorino, J.G. (2006). Acyl coenzyme A-binding protein augments bid-induced mitochondrial damage and cell death by activating mu-calpain. J. Biol. Chem. 281, 30824–30833.

Simon, C.M., Sharif, S., Tan, R.P., and LaPlaca, M.C. (2009). Spinal cord contusion causes acute plasma membrane damage. J. Neurotrauma 26, 563–574.

Stys, P.K. (2004). White matter injury mechanisms. Curr. Mol. Med. 4, 113–130.

Sun, W., Smith, D., Fu, Y., Cheng, J.X., Bryn, S., Borgens, R., and Shi, R. (2010). Novel potassium channel blocker, 4-AP-3-MeOH, inhibits fast potassium channels and restores axonal conduction in injured guinea pig spinal cord white matter. J. Neurophysiol. 103, 469–478.

Susuki, K., and Rasband, M.N. (2008). Spectrin and ankyrin-based cytoskeletons at polarized domains in myelinated axons. Exp. Biol. Med. (Maywood) 233, 394–400.

Totoiu, M.O., and Keirstead, H.S. (2005). Spinal cord injury is accompanied by chronic progressive demyelination. J. Comp. Neurol. 486, 373–383.

Vabnick, I., and Shrager, P. (1998). Ion channel redistribution and function during development of the myelinated axon. J. Neurobiol. 37, 80–96.

Wang, H., Fu, Y., Zickmund, P., Shi, R., and Cheng, J.X. (2005). Coherent anti-stokes Raman scattering imaging of axonal myelin in live spinal tissues. Biophys. J. 89, 581–591.

Waxman, S.G. (1989). Demyelination in spinal cord injury. J. Neurol. Sci. 91, 1–14.

Yamaura, I., Yone, K., Nakahara, S., Nagamine, T., Baba, H., Uchida, K., and Komiya, S. (2002). Mechanism of destructive pathologic changes in the spinal cord under chronic mechanical compression. Spine (Phila. Pa. 1976) 27, 21–26.

Address correspondence to:
Riyi Shi, M.D., Ph.D.
Department of Basic Medical Sciences
Weldon School of Biomedical Engineering
Purdue University
West Lafayette, IN 47907

E-mail: riyi@purdue.edu

or

Peng Cao, M.D., Ph.D.
Department of Orthopedics
Rui-Jin Hospital
School of Medicine
Shanghai Jiao-tong University
Shanghai, China 20025

E-mail: caopeng8@yahoo.com.cn